RESEARCH PAPER

Numerical simulation of WAAM process by a GMAW weld pool model

Y. Ogino[1] · S. Asai[1] · Y. Hirata[1]

Abstract

Additive manufacturing (AM) is a high-productivity process which can make a near-net-shape structure. In this study, the focus is the wire-arc AM (WAAM) process. In the WAAM process, wire is the depositing material. The wire melts by an arc plasma and deposits layer by layer. To establish an advanced WAAM process, it is important to make a precise structure of the intended shape. In this study, a gas metal arc welding (GMAW) weld pool model is applied to WAAM process, and influence of the deposit condition on the shape of the deposition is numerically investigated. Firstly, influence of the interpass temperature is investigated. When cooling time is set appropriately, the deposition shape becomes higher and thinner. In addition, concerning influence of the welding direction, when the welding direction is reversed for each layer, the variance of the deposition height becomes small. These numerical results show that it is important to manage the temperature and torch motion for controlling the deposition shape. These numerical results have similar tendency with experimental results and show the GMAW weld pool model is a helpful tool to predict and control the WAAM process.

Keywords Additive manufacturing · WAAM process · Numerical simulation · Weld pool model · Bead formation

1 Introduction

In recent years, the additive manufacturing (AM) process has received much attention as a high-productivity process for constructing structures. Especially, an advanced AM process for metallic material is demanded. Because the AM can produce a near-net-shape structure, the process can achieve high yield and reduce manufacturing time. Therefore, the AM process is being applied to not only rapid prototyping but also rapid manufacturing.

In the AM process, a 3D structure can be obtained by overlapping many thin layers. AM processes can be classified according to the material or the energy source used [1, 2]. Figure 1 shows some examples of AM processes. In this study, we focus on wire-arc additive manufacturing (WAAM) [3–5].

In the WAAM process, wire is the depositing material. When the wire is used as an electrode of arc discharge, the principle of the process is the same as that in gas metal arc welding (GMAW), in which the wire melts by heat input from an arc plasma This process is suitable to construct large-scale structures, and the cost of the equipment is less than that for AM processes using a laser or an electron beam. In addition, wire material can generally be handled more easily than powder material. Many studies about WAAM processes have been reported. These studies include, for example, modeling of the deposition shape [6], observation of the microstructure and the mechanical properties of the deposition [7], monitoring and controlling the deposition shape [8, 9], numerical simulation of the residual stress and the distortion in the construction [10–13], and numerical simulation of the temperature and flow field of the molten metal during the process [14].

To construct a high-quality deposition, it is very important to understand the metallurgical properties and the performance of the construction, but we think the most important issue is to obtain deposition of the intended shape without defects. To address this issue, the WAAM process, in other words, the arc welding process has to be controlled appropriately, and the relation between the welding conditions and the welding result must be understood quantitatively.

✉ Y. Ogino
ogino@mapse.eng.osaka-u.ac.jp

1   Graduate School of Engineering, Osaka University, 2-1 Yamada-oka, Suita, Osaka, Japan

Fig. 1 Schematic images of additive manufacturing systems. **a** Powder bed system. **b** Powder feed system. **c** Wire feed system

(a) Powder bed system   (b) Powder feed system   (c) Wire feed system
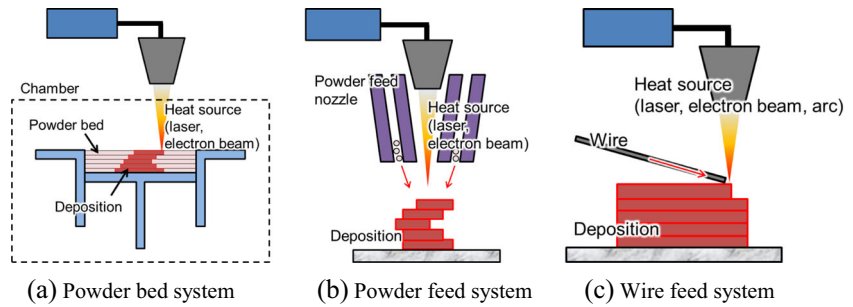
In this study, a GMAW weld pool model is applied to the WAAM process, and the influence of the deposition procedure on the deposition shape is numerically investigated. In this report, the cooling between passes and the welding direction of the layers are the primary conditions of interest. To verify the simulation results, WAAM experiments are also carried out by using a welding robot.

2 Simulation model

In this study, a GMAW weld pool model which considers flow fields and surface deformation of the molten metal is constructed [14]. In this model, heat input from the arc plasma is treated as the input from a simplified heat source model. The velocity and pressure distribution of the molten metal are calculated by the following equations:

$$\nabla \cdot \overrightarrow{v} = 0 \tag{1}$$

$$\frac{\partial \overrightarrow{v}}{\partial t} + \nabla \cdot \left(\overrightarrow{v}\, \overrightarrow{v} \right) = -\frac{1}{\rho}\nabla P + \frac{1}{\rho}\nabla\cdot\boldsymbol{\tau} + \overrightarrow{g} + \frac{1}{\rho}\overrightarrow{F}_{ex} \tag{2}$$

where $\overrightarrow{v}$ is the velocity [m/s], t is the time [s], ρ is the density [kg/m^3], P is the pressure [Pa], $\boldsymbol{\tau}$ is the viscous stress tensor [Pa], $\overrightarrow{g}$ is the acceleration of the gravity [m/s^2], and $\overrightarrow{F}_{ex}$ is the external force of the flow [N/m^3]. The equations are solved by the simplified marker-and-cell (SMAC) method [15]. The surface tension and the arc pressure, which is given by the simplified heat source model, are included as external forces. To avoid complexity, the temperature dependence of the surface tension is ignored. The surface shape of the molten metal is changed according to the velocity distribution calculated by the above equations. In this model, the surface shape of the

molten metal is tracked by the volume-of-fluid (VOF) method [16]. In the VOF method, the surface shape is described by the volume fraction of the metal (F value) in the calculation cell. The time variation of the F value is calculated by the following equation:

$$\frac{\partial F}{\partial t} + \left(\overrightarrow{v}\cdot\nabla \right) F = \Delta F \tag{3}$$

where ΔF is the source term of the F value by droplet. The temperature field in the metal is calculated by the energy conservation equation:

$$\frac{\partial H}{\partial t} + \nabla\cdot\overrightarrow{v}H = -\frac{1}{\rho}\nabla\cdot(-\kappa\nabla T) + \frac{1}{\rho}W \tag{4}$$

where H is the enthalpy [J/kg], κ is the thermal conductivity [W/mK], T is the temperature [K], and W is the source term of the energy [W/m^3]. The source term of the energy is calculated from the heat input density given by the simplified heat source model.

Next, the simplified heat source model is explained. The characteristics of the arc plasma and the droplet are described by the heat source model. Heat input density q_{arc} [W/m^2] and arc pressure p_{arc} [Pa] distributions are given by the simplified model. These distributions are Gaussian distributions, shown in Fig. 2a. Heat input from the arc plasma Q_{arc} [W], radius of the heat input r_Q [m], peak value of the arc pressure P_{arc} [Pa], and radius of the arc pressure r_P [m] are given as simplified heat source parameters, and their distributions are in terms of distance from the center of the heat source r [m], as follows:

$$q_{arc} = \frac{3Q_{arc}}{\pi r_Q^2}\exp\left(\frac{-3r^2}{r_Q^2}\right) \tag{5}$$

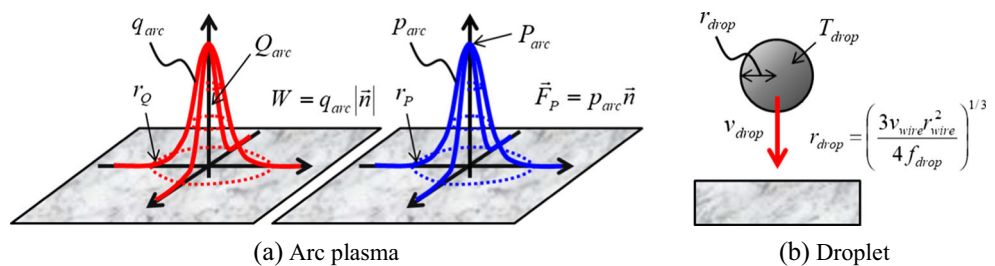**Fig. 2** Schematic images of heat source model. **a** Arc plasma. **b** Droplet

$$W = q_{arc}|\vec{n}| \qquad \vec{F}_P = p_{arc}\vec{n} \qquad r_{drop} = \left(\frac{3v_{wire}r_{wire}^2}{4f_{drop}} \right)^{1/3}$$

(a) Arc plasma   (b) Droplet

Table 1 Physical properties of mild steel

Density [kg/m³]	7200
Viscosity [Pas]	6×10^{-3}
Thermal conductivity [W/mK]	26–52
Specific heat [J/kgK]	695–800
Surface tension [N/m]	1.2
Melting temperature [K]	1750
Latent heat of fusion [J/kg]	2.47×10^5

$$p_{arc} = P_{arc} \exp\left(\frac{-3r^2}{r_P^2}\right) \qquad (6)$$

These values are converted to volumetric values by multiplying the normal vector $\overrightarrow{n}$ [1/m] and substituting them into Eqs. (2) and (4). Here, the normal vector is calculated by the following equation:

$$\overrightarrow{n} = \nabla F \qquad (7)$$

The simplified droplet is a sphere shape, shown in Fig. 2b. The radius of the droplet r_{drop} [m] is determined by the wire radius r_{wire} [m], wire feeding rate v_{wire} [m/s], and the frequency of the droplet transfer f_{drop} [Hz]. The droplet is injected onto the base metal according to the frequency. In this model, the droplet keeps the constant droplet velocity v_{drop} [m/s] and the constant droplet temperature T_{drop} [K] until it touches the base metal. To express the experimental results by this model quantitatively, the abovementioned heat source parameters must be adjusted to obtain a similar bead shape in advance. In this study, the droplet and the base metal are mild steel for both the simulations and the experiments. The material properties of the steel are shown in Table 1 [17, 18]. The boundary at the surface of the weld pool and the base metal is set thermal insulation for energy transport and open boundary for flow field.
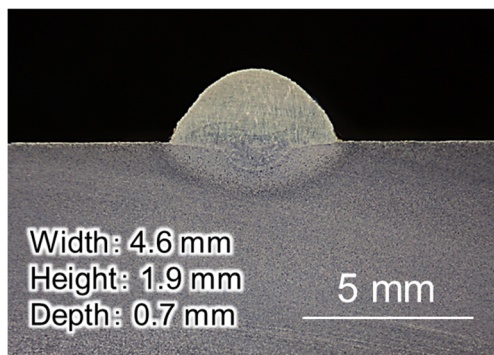

Fig. 3 Cross-sectional shape of penetration in experiments (wire feed rate 300 cm/min, welding speed 60 cm/min, CTWD 15 mm)

3 Experimental equipment and standard condition

In this study, the cold metal transfer (CMT) process, which can conduct welding with a low heat input, is used in the experiments. The power source is TranPuls Synergic 3200 (Fronius) and the wire feeding machine is VR 7000 CMT (Fronius). The welding torch is fixed at the welding robot, and the weld bead is formed on the base metal layer by layer. The welding wire is mild steel, and the shielding gas is Ar + 20%CO_2 (flow rate: 20 L/min). Before carrying out the WAAM experiments, a bead-on-plate welding test was conducted to select the welding conditions. We selected a wire feeding rate of 300 cm/min, a welding speed of 60 cm/min, and a contact-tip-to-work distance (CTWD) of 15 mm as the standard condition in all experiments. In this condition, the arc current is about 110 A, and the welding voltage is about 15 V. By using this standard condition, a stable thin bead is obtained. The cross-section of the weld bead by using the standard condition is shown in Fig. 3.

4 Determination of the simplified heat source parameters used in simulations

The simplified heat source parameters used in the simulation model are adjusted so that the bead shape calculated by the model agrees with those of the experimental result shown in Fig. 3. The heat source parameters are shown in Table 2, and the bead shape of the numerical result is shown in Fig. 4. Here, we referred the arc current and the welding voltage of experiment to set the value of the heat input. Bead width, bead height, and penetration depth of the numerical result are similar to those of the experiment. These heat source parameters are used in all simulations.

Table 2 Heat source parameters used in this study

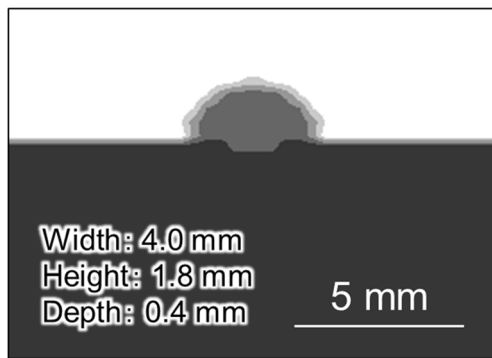|	
Heat input [W]	1440
Radius of heat input distribution [mm]	5.0
Peak of arc pressure [Pa]	1000
Radius of arc pressure distribution [mm]	5.0
Wire radius [mm]	0.6
Wire feeding rate [cm/min]	300
Transfer frequency of droplet [Hz]	100
Droplet temperature [K]	2500
Droplet velocity [cm/s]	20
Welding speed [cm/min]	60

Fig. 4 Simulation result of cross-sectional shape

5 Simulations and experiments of the WAAM process

5.1 Influence of the interpass temperature

The numerical model is applied to the WAAM process and the results obtained are shown. First, the influence of cooling between weld passes is numerically investigated. Figure 5 shows the heat source motion used in the simulation. In this simulation, the deposition shape is a linear shape. At the first pass, the target position is the surface of the base metal, and the heat source moves from the start position (position A) to the end position (position B). The distance from position A to B is set to 50 mm. At the second pass, the heat source moves 1.5 mm upward from the previous start position (position C) to the end position (position D). In this simulation, the number of welding layers is 10. Here, two kinds of cooling conditions are numerically investigated. First, no cooling time is given between weld passes (cooling condition A). In this case, welding starts just after the previous layer is welded. Second, the weld bead is cooled after every pass (cooling condition B). The temperature of the metal is reset at 300 K after all of the metal in the calculation domain is solidified.
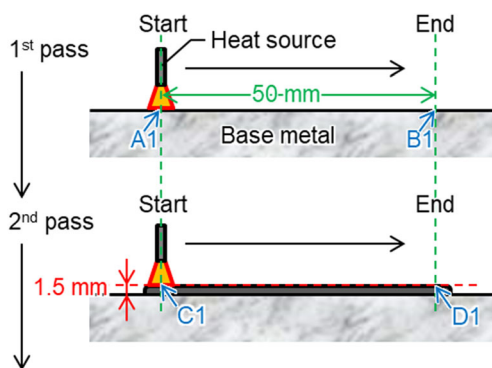

Fig. 5 Schematic image of motion of heat source in first simulation

Figure 6 shows the numerical results of the deposition shape and its cross-section at the center of the weld bead. As shown in this figure, when cooling between the weld passes is given, the deposition shape becomes thinner and higher than that without cooling. In the case of the passes without cooling the temperature of the welding object is higher and the deposition easily melts and breaks down by gravity force. Therefore, in order to control the deposition shape, it is very important to manage the temperature of the object throughout the entire welding process.

To verify the numerical results, experiments are carried out. The motion of the welding torch is shown in Fig. 7. The number of layers is 40, and the length of the passes is 100 mm. To investigate the influence of cooling, two conditions are compared. First, no cooling time is given between welding passes. Second, the welding robot is suspended between passes until the temperature of the deposition surface becomes 573 K. The temperature of the deposition is measured by a surface thermometer at the start position of the next welding.

The experimental results of the deposition shape are shown in Fig. 8. The welding direction is from the left-hand side to the right-hand side. As shown in the figure, the deposition shape becomes higher when the cooling time is considered between the passes. Additionally, the surface roughness of the deposition is smaller in this case. Therefore, the deposition shape depends on the interpass temperature, and it has to be set appropriately in order to obtain a higher and thinner deposition. The experimental results and the numerical results indicate a similar tendency. Hereafter, in this report, the welding robot is suspended when the temperature of the deposition becomes 573 K between every pass as a cooling condition to obtain the deposition stably in the experiments.

5.2 Influence of welding direction in linear shape WAAM

As shown in Figs. 6 and 8, the deposition shape is higher at the start position of welding and lower at the end position. Here, the influence of welding direction is investigated for achieving less variation of the deposition height in a structure of linear ("L") shape.

In this section, two kinds of welding directions are considered, as shown in Fig. 9. First, the start and the end positions of every welding pass are overlapped and the welding direction is the same in every pass, as shown in Fig. 9a (Pattern L-A). Second, the welding starts at the end position of the previous pass, and the welding direction is reversed for each layer, as shown in Fig. 9b (Pattern L-B). The number of layers is 10 and the welding length is 50 mm. In this simulation, if it is assumed that the deposition temperature becomes sufficiently

Fig. 6 Numerical results for influence of the cooling condition on the deposition shape. **a** Cooling condition A (without cooling), (i) deposition appearance, (ii) cross-section. **b** Cooling condition B (with cooling), (i) deposition appearance, (ii) cross-section

(i) Deposition appearance　　　　　(ii) Cross-section

(a) Cooling condition A (without cooling)

(i) Deposition appearance　　　　　(ii) Cross-section

(b) Cooling condition B (with cooling)
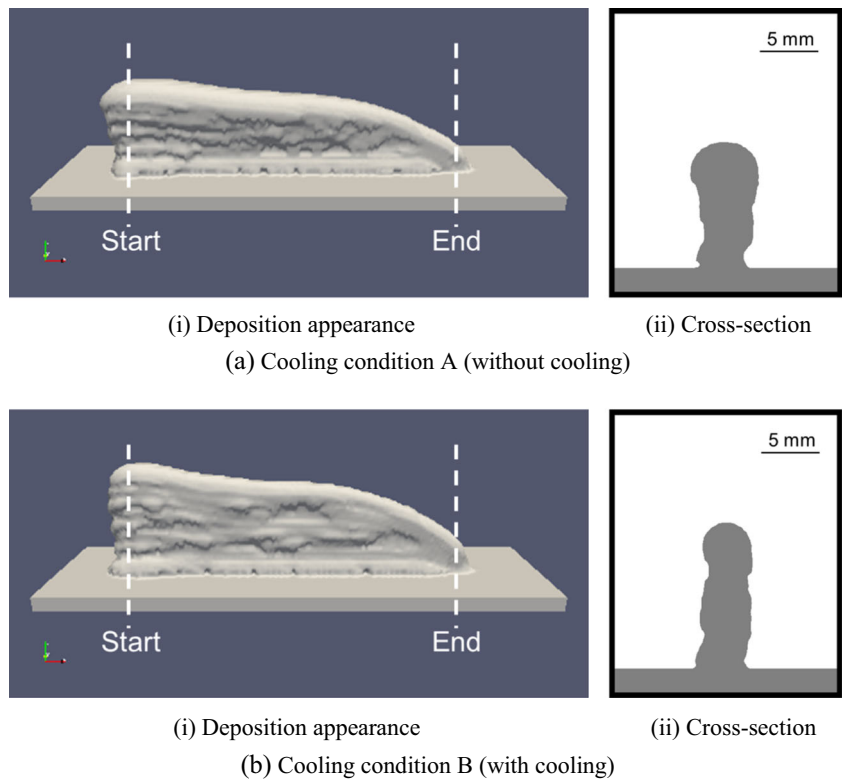
low at every pass, the temperature of the metal is 300 K after all of the metal in the calculation domain is solidified.

Figure 10 shows the simulation results of the deposition shape. As shown in the figure, when the welding direction is
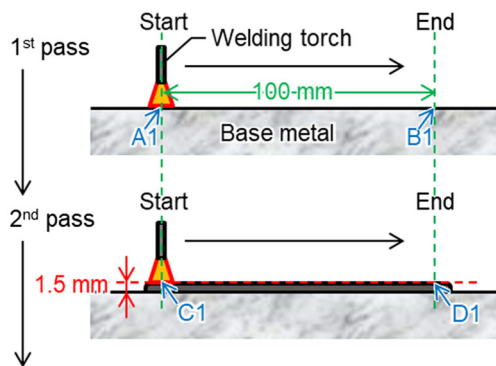
Fig. 7 Schematic images of welding torch motion in experiments

Fig. 8 Experimental results of the deposition shape depending on the cooling condition. **a** No management, **b** Waiting until 573 K

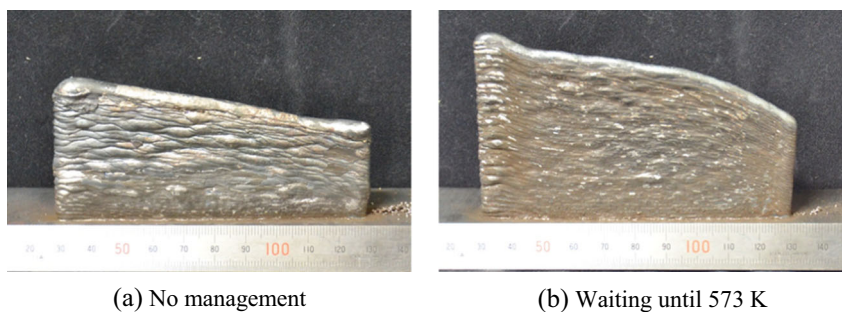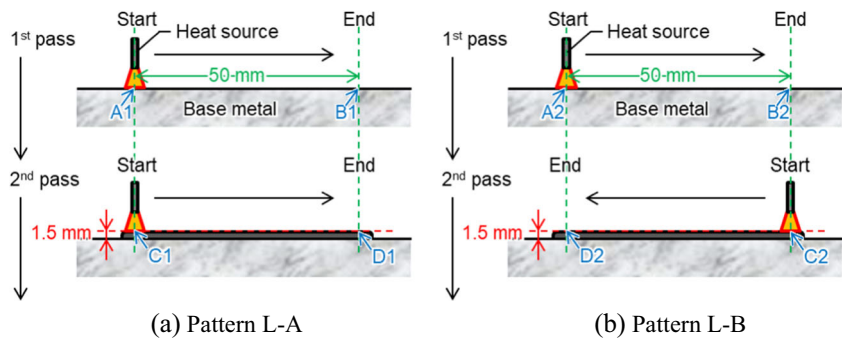reversed for each layer, the variation of the deposition height is suppressed. In the welding process, the start edge of the bead tends to higher than the end edge. At the start position, the temperature of the base metal low and the molten metal solidifies rapidly and not spreads. In addition, since the molten metal flows to the backward of the welding torch, the bead height becomes low at the end position. When the torch motion is reversed for each layer, these effects are canceled layer by layer, and the variation of the deposition height is suppressed. To control the deposition shape, it is preferable to have small height variation, and so it is important to set the welding direction appropriately.

Next, the experimental results are shown. The motion of the welding torch is shown in Fig. 11. The welding length is 100 mm, and the number of layers is 40. Figure 12 shows the experimental results of the deposition shape. Figure 12a has already been shown in Fig. 8b, but for comparison, it is shown again here. As shown in Fig. 12, the variation of the deposition

(a) No management　　　　　　　(b) Waiting until 573 K

Fig. 9 Schematic images of heat source motion for linear shape deposition in simulations. (a) Pattern L-A. (b) Pattern L-B

(a) Pattern L-A   (b) Pattern L-B

height is significantly suppressed in the case of the welding direction reversed for each layer. The experimental results and the numerical results show similar tendencies.

5.3 Influence of welding procedure in cylindrical shape WAAM

In this section, the influence of the welding procedure on a cylindrical shape ("C") deposition is discussed by simulations and experiments. The start position of the weld pass and its end position are overlapped in every layer differently from the

case of linear shape deposition. Here, three kinds of welding procedures are compared. The heat source motion used in the simulation is shown in Fig. 13. In the first case, the start position is the same and the direction of the torch motion is also the same, as shown in Fig. 13a (Pattern C-A). In the second case, the start position is the same, but the direction of the torch motion is reversed for each layer, as shown in Fig. 13b (Pattern C-B). In the third case, the direction of the torch motion is the same, but the start positon is changed layer by layer, as shown in Fig. 13c (Pattern C-C). In Pattern C-C, the shift amount is set to 180° per one layer. In

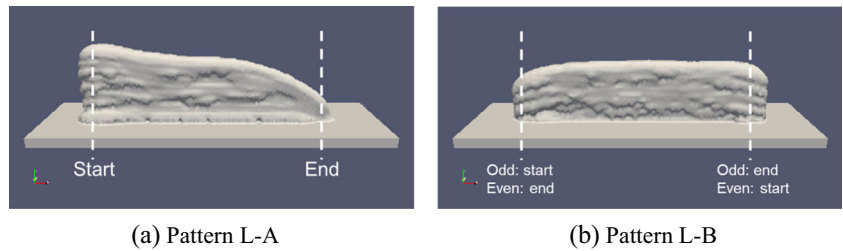Fig. 10 Numerical results of the deposition shape with different welding directions. a Pattern L-A. b Pattern L-B

(a) Pattern L-A   (b) Pattern L-B

Fig. 11 Schematic images of welding torch motion for investigating the influence of the welding direction. a Pattern L-A. b Pattern L-B
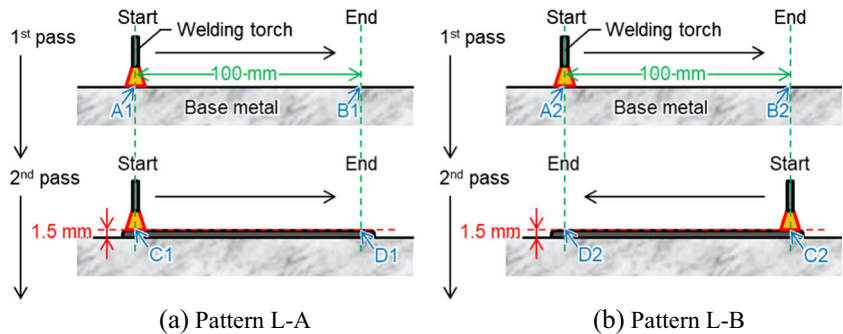

(a) Pattern L-A   (b) Pattern L-B

Fig. 12 Experimental results of the deposition shape with different welding directions. a Pattern L-A. b Pattern L-B

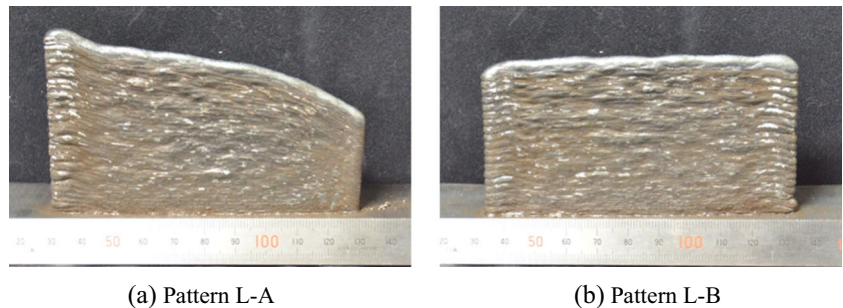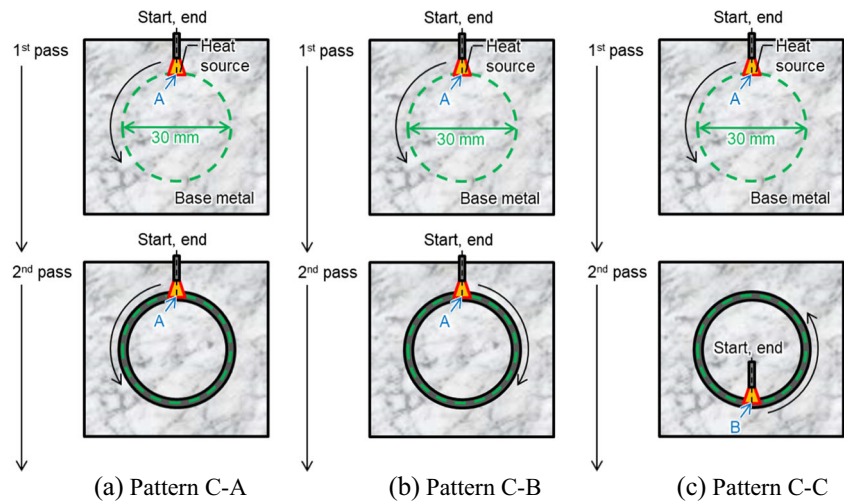(a) Pattern L-A   (b) Pattern L-B

Fig. 13 Schematic images of torch motion for cylindrical shape deposition in simulations. **a** Pattern C-A. **b** Pattern C-B. **c** Pattern C-C

(a) Pattern C-A   (b) Pattern C-B   (c) Pattern C-C

the simulation, the diameter of the cylinder is set to 30 mm, the number of layers is 10 and the heat source moves 1.5-mm upward layer by layer. Here, as in the simulation described in Section 5.2, the temperature of the metal is reset at 300 K after all of the metal in the calculation domain has solidified.

Figure 14 shows the numerical results of the deposition shape. Points A and B correspond with points A and B in Fig. 13. As shown in Fig. 14, in the case of Pattern C-A, the height of the deposition becomes higher at the start position of welding. As shown in Fig. 14b, the direction of the torch

motion is reversed for each layer, and the variation of the height of the deposition is suppressed. Even though the start position is changed layer by layer, the height of the deposition at the start position becomes higher, as shown in Fig. 14c. These simulation results show that the direction of the torch motion is important to obtain a height-wise uniform deposition for cylindrical shapes. This result shows the same tendency as in the linear shape deposition.

Next, an experiment is carried out. The torch motion is shown in Fig. 15. The diameter of the cylinder is 50 mm, and the number of layers is 40.

Fig. 14 Numerical results for cylindrical shape deposition. **a** Pattern C-A. **b** Pattern C-B. **c** Pattern C-C
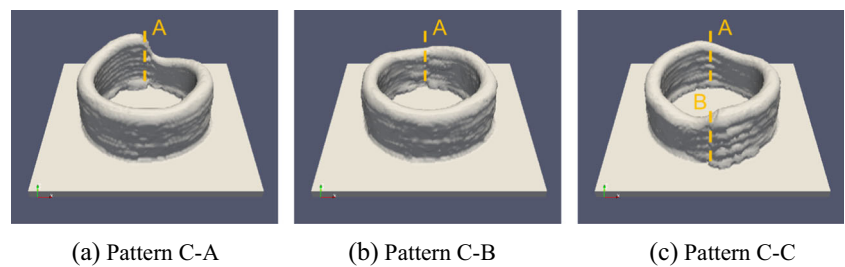

(a) Pattern C-A   (b) Pattern C-B   (c) Pattern C-C

Fig. 15 Schematic images of the torch motion for cylindrical shape deposition in experiments. **a** Pattern C-A. **b** Pattern C-B. **c** Pattern C-C
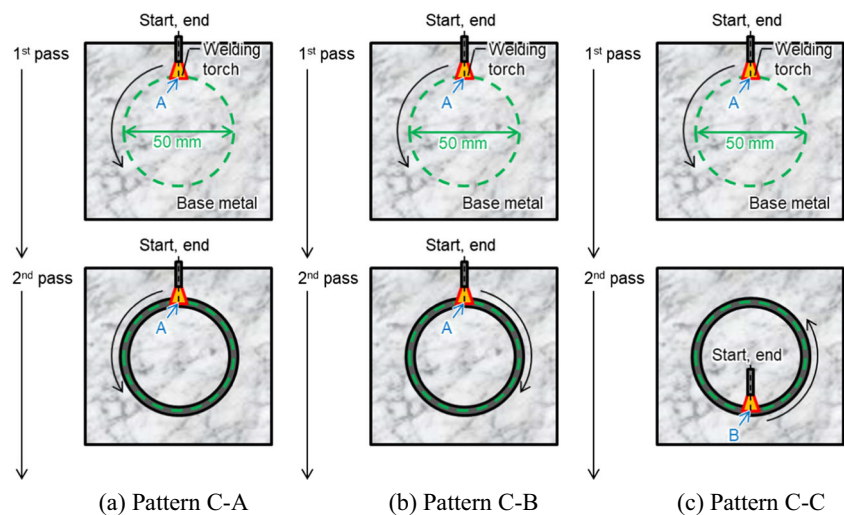

(a) Pattern C-A   (b) Pattern C-B   (c) Pattern C-C

Fig. 16 Experimental deposition results for cylindrical shape deposition. **a** Pattern C-A. **b** Pattern C-B. **c** Pattern C-C

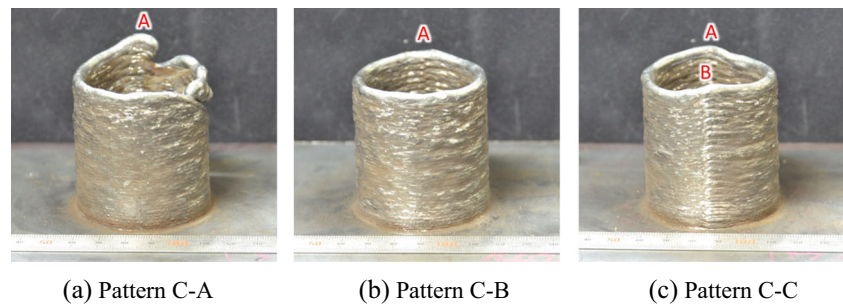(a) Pattern C-A   (b) Pattern C-B   (c) Pattern C-C

Figure 16 shows the experimental results. Points A and B corresponds with points A and B shown in Fig. 15. As shown in Fig. 16a, the top shape of the deposition is broken when the welding procedure is Pattern C-A. On the other hand, in the case of Pattern C-B, the height of the deposition becomes uniform, as shown in Fig. 16b. In the case of Pattern C-C, shown in Fig. 16c, the height of the deposition becomes higher at the start position. The experimental results and the numerical results show a similar tendency.

In this study, because the size of the deposition is different between the simulations and the experiments, it is difficult to compare their results quantitatively, but both sets of results show a similar tendency depending on the cooling condition or welding direction. Therefore, this study shows the possibility of realizing high-productivity and high-quality WAAM processes by using simulations. In addition, to improve the accuracy of the simulation result and understand the phenomena in the WAAM process more deeply, it is required to make clear the influence of the important factors such as the behavior of the arc plasma and the driving force on the molten metal, by enhancement of the simulation model.

6 Conclusion

In this study, a GMAW weld pool model is applied in a WAAM process. The influences of cooling between passes and the welding direction are numerically and experimentally investigated. The results obtained are summarized as follows:

(1) The deposition shape becomes higher and thinner under the appropriate cooling condition.
(2) In the case of linear shape deposition, the height of the deposition becomes uniform when the direction of the torch motion is reversed for each layer.
(3) In the case of cylindrical shape deposition, the welding direction is also important for obtaining height-wise uniform deposition.
(4) Although the scale of deposition differs between the simulations and the experiments, the results show a similar tendency depending on the condition. Therefore, the simulation model can be a helpful tool for realizing high-productivity and high-quality WAAM processes.

References

1. Frazier WE (2014) Metal additive manufacturing: a review. J Mater Eng Perform 23(6):1917–1928
2. Ding D, Pan Z, Culuri D, Li H (2015) Wire-feed additive manufacturing of metal components: technologies, developments and future interests. Int J Adv Manuf Technol 81(1-4):465–481. https://doi.org/10.1007/s00170-015-7077-3
3. Williams SW, Martina F, Addison AC, Ding J, Pardal G, Colegrove P (2016) Wire + arc additive manufacturing. Mater Sci Technol 32(7):641–647. https://doi.org/10.1179/1743284715Y.0000000073
4. Martina F, Mehnen J, Williams SW, Colegrove P, Wang F (2012) Investigation of the benefits of plasma deposition for the additive layer manufacturing of Ti-6Al-4V. J Mater Process Technol 212(6):1377–1386. https://doi.org/10.1016/j.jmatprotec.2012.02.002
5. Katou M, Oh J, Miyamoto Y, Matsuura K, Kudoh M (2007) Freeform fabrication of titanium metal and intermetallic alloys by three-dimensional micro welding. Mater Des 28(7):2093–2098. https://doi.org/10.1016/j.matdes.2006.05.024
6. Suryakumar S, Karunakaran KP, Bernard A, Chandrasekhar U, Raghavender N (2011) Weld bead modeling and process optimization in hybrid layered manufacturing. Comput Aided Des 43(4):331–344. https://doi.org/10.1016/j.cad.2011.01.006
7. Wang F, Williams S, Colegrove P, Antonysamy AA (2013) Microstructure and mechanical properties of wire and arc additive manufactured Ti-6Al-4V. Metall Mater Trans A 44A:968–977
8. Xiong J, Zhang G (2014) Adaptive control of deposited height in GMAW-based layer additive manufacturing. J Mater Process Technol 214(4):962–968. https://doi.org/10.1016/j.jmatprotec.2013.11.014
9. Xiong J, Zhang G, Zhang W (2015) Forming appearance analysis in multi-layer single-pass GMAW-based additive manufacturing. Int J Adv Manuf Technol 80(9-12):1767–1776. https://doi.org/10.1007/s00170-015-7112-4
10. Zhao H, Zhang G, Yin Z, Wu L (2011) A 3D dynamic analysis of thermal behavior during single-pass multi-layer weld-based rapid prototyping. J Mater Process Technol 211(3):488–495. https://doi.org/10.1016/j.jmatprotec.2010.11.002
11. J. Ding, P. Colegrove, J. Mehnen, S. Ganguly, P.M. Sequeira Almeida, F. Wangb and S. Williams, Thermo-mechanical analysis of wire and arc additive layer manufacturing process on large multi-layer parts, Computation Material Science, 50 (2011), 3315–3322
12. Zhao H, Zhang G, Yin Z, Wu L (2012) Three-dimensional finite element analysis of thermal stress in single-pass multi-layer weld-based rapid prototyping. J Mater Process Technol 212(1):276–285. https://doi.org/10.1016/j.jmatprotec.2011.09.012

13. Zhou X, Zhang H, Wang G, Bai X (2016) Three-dimentional numerical simulation of arc and metal transport in arc welding based additive manufacturing. Int J Heat Mass Transf 103:521–537. https://doi.org/10.1016/j.ijheatmasstransfer.2016.06.084

14. Ogino Y, Takabe Y, Hirata Y, Asai S (2017) Numerical model of weld pool phenomena with various joint geometries and welding position. Q J Jpn Weld Soc 35(1):13–20 (in Japanese)

15. Amsden AA and Harlow FH (1970) The SMAC method: a numerical technique for calculating incompressible fluid flows, Los Alamos science laboratory report, LA-4370

16. Hirt CW, Nichols BD (1981) Volume of fluid (VOF) method for the dynamics of free boundaries. J Comput Phys 39(1):201–225. https://doi.org/10.1016/0021-9991(81)90145-5

17. Rao ZH, Hu J, Liao SM, Tsai HL (2010) Modeling of the transport phenomena in GMAW using argon–helium mixtures. Part I—the arc. Int J Heat Mass Transf 53(25-26):5707–5721. https://doi.org/10.1016/j.ijheatmasstransfer.2010.08.009

18. Ushio M, Wu CS (1997) Mathematical modeling of three-dimensional heat and fluid flow in a moving gas metal arc weld pool. Metall Mater Trans B 28B:509–516